buildings

MDPI

Article

Durability Deterioration of Geopolymer Stabilized Soft Soil under Sodium Sulfate and Magnesium Sulfate Attack: A Comparative Study

Xinxiang Yi [1,2], Guanci Wang [1,2], Benben Zhang [2,*], Genbao Zhang [3,*], Yuming Liu [2,4] and Zhengdong Luo [2]

[1] Yueyang Road and Bridge Group Co., Ltd., Yueyang 414000, China
[2] College of Civil Engineering, Xiangtan University, Xiangtan 411105, China
[3] College of Civil Engineering, Hunan City University, Yiyang 413000, China
[4] Hengyang Highway and Bridge Construction Co., Ltd., Hengyang 421001, China
* Correspondence: zhangbenben@smail.xtu.edu.cn (B.Z.); genbao@hncu.edu.cn (G.Z.)

Abstract: Sulfate attack is one of the non-negligible factors that induces deterioration in the performance and life cycle of soil stabilizers. In this paper, the degradation mechanism of the durability of slag–fly-ash-based geopolymer stabilized soft soil (hitherto referred to as SF-GSSS) under the sodium sulfate (Na_2SO_4) and magnesium sulfate ($MgSO_4$) attack environment is comparatively investigated, and the slag/fly ash ratios are set to S10F0, S9F1, S8F2, and S7F3. The SF-GSSS was fully immersed in a 2.5% Na_2SO_4 solution and 2.5% $MgSO_4$ solution, respectively, to characterize the deterioration rules via visual observations, an unconfined compressive strength (UCS) test, and by mass change. The effect of sulfate on the microstructural characteristics of the SF-GSSS were determined by different microanalytical means, such as by X-ray diffraction (XRD) and scanning electron microscopy (SEM). The results showed that the SF-GSSS immersed in a $MgSO_4$ solution displayed significant physical deterioration, but not when in a Na_2SO_4 solution. The mass growth of the SF-GSSS when immersed in a Na_2SO_4 solution was significantly lower than when it was immersed in a $MgSO_4$ solution at the same immersion age. The rate of strength loss was lowest for S9F1 and highest for S7F3 at the end of immersion, regardless of its immersion in Na_2SO_4 or $MgSO_4$ solutions.

Keywords: geopolymer; slag–fly ash; soft soil stabilization; durability; sulfate attack

Citation: Yi, X.; Wang, G.; Zhang, B.; Zhang, G.; Liu, Y.; Luo, Z. Durability Deterioration of Geopolymer Stabilized Soft Soil under Sodium Sulfate and Magnesium Sulfate Attack: A Comparative Study. *Buildings* **2023**, *13*, 1075. https://doi.org/10.3390/buildings13041075

Academic Editor: Jan Fořt

Received: 7 March 2023
Revised: 10 April 2023
Accepted: 17 April 2023
Published: 19 April 2023

1. Introduction

Over the years—in the construction of high-speed railways, highways, dams, airports, and other infrastructures—various special foundations are often crossed, among which soft-soil foundation is the most common. As a kind of special soil, soft soil is characterized by a high natural moisture content, high compressibility, poor mechanical properties, and high fluidity, which makes it easy for it to cause engineering problems, such as uneven settlement and foundation instability, in the construction facilities located above it [1]. Therefore, soft-soil foundations often need to be pre-reinforced by certain foundation treatment techniques. Due to the advantages of high construction efficiency, good reinforcement effect, and low engineering cost, chemically stabilized soil technology has been widely used in engineering. Chemically stabilized soil technology refers to the injection of soil stabilizer into the soil to be treated, which improves the macroscopic mechanical properties and the different aspects of durability of the in situ soil through physicochemical action [2,3]. Currently, the most commonly used soil stabilizer is cement. However, the cement-stabilized soil generally suffers from the disadvantages of easy cracking, high dry shrinkage, insufficient early strength, and poor durability [4]. In addition to the above-mentioned problems, the excessive use of cement also tends to cause ecological troubles. The process of cement preparation consumes excessive non-renewable resources, emits plenty of CO_2, and small amounts of dust, which inevitably increases the burden on the

ecological environment, threatens the health of the surrounding residents, and is not in line with the sustainable development of human society [5–7]. Therefore, it is economically and ecologically important to develop a green, sustainable, low-carbon, and energy-saving soil stabilization agent that can replace cement.

Geopolymer is a class of structurally stable inorganic gelling substance formed by an amorphous aluminosilicate compound with potential gelation activity as a precursor after depolycondesation and polycondensation reactions under the action of an alkali activator [8]. Most of these precursors come from solid wastes generated from industrial production processes, the most common of which are slag, fly ash, and metakaolin. Previous indoor experimental studies have confirmed that geopolymer has the advantages of high early strength, fast setting and hardening, relatively good resistance to various types of chemical ions, and a strong ability to sequester heavy metal ions when compared to traditional cement-based cementitious materials [9–11]. In addition, since geopolymer is produced and prepared without calcination, it has the characteristics of low production energy consumption and low CO_2 emissions [12]. The CO_2 emissions and energy consumption is 10–20% for geopolymer and 60% for cement, respectively, under the same production technology conditions [13,14]. It can be seen that geopolymer is an ideal substitute for cement.

At present, scholars have successfully demonstrated the implementability of applying geopolymer to the field of various types of soil stabilization and have achieved fruitful results. Sahoo et al. [15] comparatively analyzed their UCS and durability performance, such as freeze–thaw cycle resistance and the water stability of expansive soil stabilized with conventional soil stabilizers (cement, lime, etc.) and slag-based geopolymers. The conclusions indicated that the geopolymer stabilized soil had superior mechanical properties when compared to conventional soil stabilizer, which was mainly attributed to the denser internal structure of geopolymer stabilized soil. Ghadir et al. [16] also reported the same findings and confirmed, from a life cycle assessment perspective, that geopolymer stabilized soil released less CO_2 and had less of an environmental impact than cement stabilized soil. Zhou et al. [17] investigated that the strength of low-calcium-type metakaolin-based geopolymer stabilized soil decreased in the early maintenance period, and had a linear increase in the later maintenance period, while the strength development pattern of high-calcium-type slag-based geopolymer stabilized soil was opposite to it. Other studies [18–20] have verified the feasibility and superiority of geopolymer stabilized soil from different perspectives, such as its mechanical properties, microstructure, and reaction mechanisms, and pointed out that geopolymer is fully capable of replacing traditional cement-based cementitious material in the field of soil stabilization.

It is well known that durability is an irreplaceable aspect in evaluating the overall performance of building structural components, which determine the life cycle of building structures. Among them, the resistance to chemical ion attack is an indispensable index in the evaluation of durability performance, where sulfate attack is more common in underground structures. At present, the research, carried out by scholars at home and abroad, on the resistance to sulfate attacks of soil stabilized by cementitious materials has mainly focused on ordinary Portland cement stabilized soil; this research has achieved some progressive results. It has been shown [21–23] that gypsum and ettringite with expansion characteristics are generated inside the ordinary Portland cement stabilized soil under sulfate attack conditions, and that the expansion stress generated in this way causes a sharp decline in the performance of the ordinary Portland cement treated soil in all aspects until it loses its load-bearing capacity completely, and it is accompanied by the occurrence of deterioration phenomena such as swelling, cracking, and spalling. Han et al. [24] and Bonen et al. [25] further found via an indoor simulated sulfate attack test that magnesium sulfate degraded ordinary Portland cement stabilized soil more severely than the attack effect of sodium sulfate. The research data showed that the stabilization mechanism of a geopolymer with a unique three-dimensional network spatial structure system, formed by the geopolymerization reaction, was significantly different from that of ordinary Portland

cement in the soil to be treated. Up to now, scholars have conducted a great deal of experimental studies on geopolymer stabilized soil in terms of macroscopic mechanical properties and microstructural characteristics, but there are fewer reports on the resistance of geopolymer stabilized soil to sulfate attack. In addition, the deterioration mechanism of sulfate on the durability of geopolymer stabilized soil is not yet clear. In view of the above deficiencies—for the sake of elucidating the influence of sulfate on the macroscopic properties and microstructure of geopolymer stabilized soil, and on the deterioration mechanism—relevant research work is urgently needed.

Therefore, the main thrust of this paper is to investigate the degradation mechanism of the durability of SF-GSSS with different slag/fly ash ratios under different sulfate solution attacks, where the slag/fly ash ratios are determined as S10F0, S9F1, S8F2, and S7F3 and the sulfate solutions are of a 2.5% Na_2SO_4 solution and 2.5% $MgSO_4$ solution. The macroscopic deterioration of SF-GSSS under sulfate attack was evaluated by visual observation, mass variation, and changes in UCS. Moreover, the alteration process of the mineral composition and microstructure of SF-GSSS were determined by different microanalytical means, such as XRD and SEM.

2. Materials and Methods

2.1. Materials

The soil sample was selected from soft soil around the Dongting Lake area in Hunan Province, China, with soil depths located at about 5 m below ground. The soft soil brought back was dried, crushed, and passed through a 2.0 mm (80 mesh) geotechnical sieve. It was then stored in geotechnical drums to ensure use for later experiments. The main physical and mechanical property indices of the soft soil are shown in Table 1.

Table 1. Main physical and mechanical property indices of the soft soil.

Soil Sample	Natural Moisture Content (%)	Specific Gravity	Liquid Limit (%)	Plastic Limit (%)	Compression Modulus (MPa)	Void Ration	Wet Density ($g \cdot cm^{-3}$)
Soft soil	50.2	2.55	49.9	25.7	3.85	1.45	1.49

In this experiment, slag and fly ash were used as precursor materials for the preparation of the geopolymer. The slag was provided by Shijiazhuang Hongyao Mineral Processing Co., Ltd., in Shijiazhuang, Hebei, China, and the fly ash was supplied by Zhengzhou Hengyuan New Materials Co., Ltd., in Zhengzhou, Henan, China. The appearance and microscopic images of the materials (soft soil, slag, and fly ash) used in the test are shown in Figure 1. It is not difficult to see that the soft soil consists of yellow soil particles with rough surfaces and more internal pores in the form of scale clusters, in which the content of particles with a size less than 0.005 mm is 32.70%, the particles with a size between 0.005 and 0.075 mm is 65.90%, and the particles with a size between 0.075 and 2.000 mm is 1.40%; the slag with a particle size of 500 mesh is white powder, its angularity is obvious, and it has an irregular polygon shape; and the fly ash with a particle size of 400 mesh is gray-black powder-like, which is composed of spherical glass beads with a smooth surface of varying diameters. The chemical mineral composition of the geopolymer precursor materials (slag and fly ash) were characterized by X-ray fluorescence spectrometry (XRF), the test results of which are shown in Table 2.

Table 2. Main chemical mineral composition of the geopolymer precursor materials (%).

	CaO	Al_2O_3	SiO_2	MgO	Fe_2O_3	SO_3	K_2O	TiO_2
Slag	35.25	16.75	34.55	5.06	1.55	1.26	-	-
Fly ash	2.34	34.72	53.10	0.88	2.55	0.37	1.78	1.27

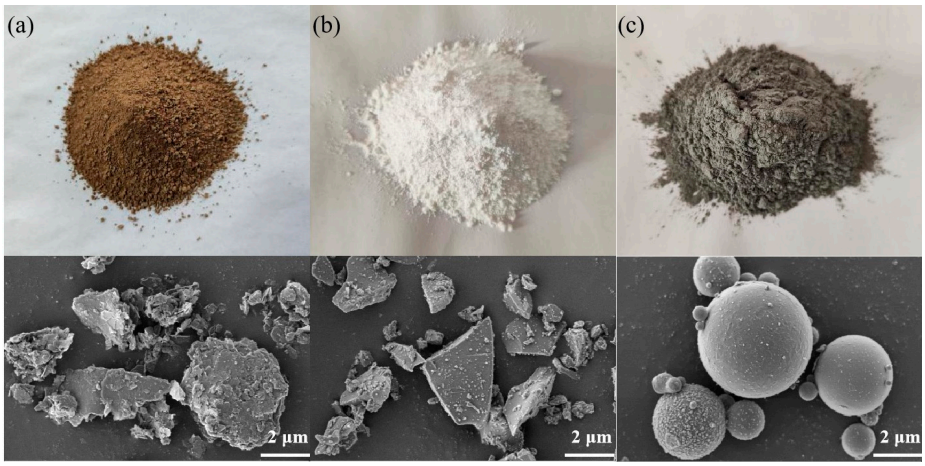

Figure 1. The appearance and microscopic images of raw materials: (**a**) soft soil; (**b**) slag; and (**c**) fly ash.

Previous experimental studies [26,27] revealed that the use of composite alkali activators produced the best activation effect on geopolymer precursor materials, especially the NaOH + Na_2SiO_3 solution, as opposed to single alkali activators such as caustic soda, alkali silicate, and alkali carbonate. In addition, the modulus of the alkali activator has an important role in influencing various aspects of the geopolymer, such as its mechanical and workability properties. Wang et al. [28] stated that the optimal control range for the modulus of alkali activators was 1.0–1.5. Therefore, in order to make this study more capable of being referenced, a NaOH + Na_2SiO_3 solution was used as the alkali activator and its modulus was set to 1.2. Both the NaOH and Na_2SiO_3 solutions used in the test were commercially available materials, as is shown in Figure 2. The NaOH was in the form of white flakes of varying shapes and was analytically pure, while the Na_2SiO_3 solution was clear and viscous with a modulus of 3.31, and contained mainly Na_2O (8.42 wt%) and SiO_2 (27.84 wt%) in the form of oxides. The alkali activator modulus was adjusted by adding 19.14 g of NaOH fragments per 100 g of Na_2SiO_3 solution.

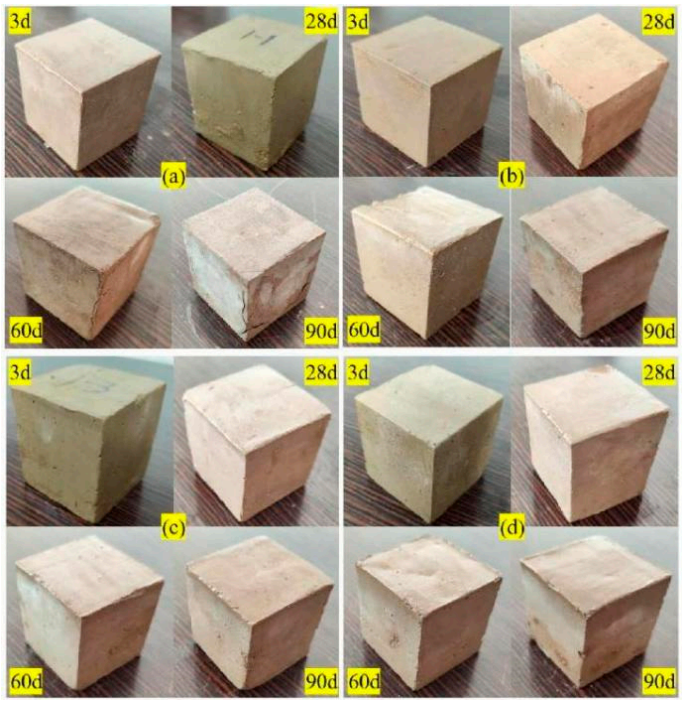

Figure 2. Visual appearance of SF-GSSS immersed in Na_2SO_4 solution: (**a**) S10F0; (**b**) S9F1; (**c**) S8F2; and (**d**) S7F3.

2.2. Specimen Preparation

The specific procedure of the experiment is shown in Table 3. With reference to the results of the preliminary preparatory tests and other studies [29,30], taking into account the conditions of mechanical properties and workability, the percentage of stabilization agent was set to 25% (the ratio of geopolymer precursors to dry soft soil in terms of mass); the percentage of alkali activator was set to 40% (the ratio of alkali activator solution to geopolymer precursors in terms of mass); and the water to cement ratio was set to 0.4 (the ratio of water to geopolymer precursors in terms of mass). The detailed steps for the sample preparations are shown below.

Table 3. Mixture design of the testing program.

Mix Codes	Precursors Content (wt%)	Slag: Fly Ash	Slag Content (wt%)	Fly Ash Content (wt%)	Alkali Activator		Water/ Precursors	Curing Age (Days)
					Modulus	Content (wt%)		
S10F0	25	10:0	25	0	1.2	40	0.4	28
S9F1	25	9:1	22.5	2.5	1.2	40	0.4	28
S8F2	25	8:2	20	5	1.2	40	0.4	28
S7F3	25	7:3	17.5	7.5	1.2	40	0.4	28

(1) The dry soil in the geotechnical drums was poured into an appropriate amount of tap water and mixed evenly to prepare the remodeled soil. It was then sealed for 24 h before use so that the water could diffuse evenly into the soil and come into complete contact with the soil particles. The moisture content of the remodeled soil was adjusted to 50.2% to match the in situ soil as closely as possible;
(2) The appropriate amount of NaOH fragments and Na_2SiO_3 solution were weighed together and poured into a magnetic stirrer. They were then stirred uniformly for the preparation of the composite alkali activator solution, which was left in the room for 24 h to come to room temperature in order to eliminate the effect of temperature on the test results;
(3) The geopolymer precursor materials (slag and fly ash) were weighed and poured into the net slurry mixer for 3 min at a slow speed. Next, the alkali activator solution and distilled water were, in turn, poured into the mixer for 2 min at a slow speed, and then 3 min at a fast speed to prepare the geopolymer slurry;
(4) The geopolymer slurry and the remodeled soil were added together into the mixing drum and mixed well to form the SF-GSSS slurry, which was then poured into the standard triplex mold (70.7 × 70.7 × 70.7 mm) three times. In addition, the surface of the sample was scraped smooth with a scraper. The air bubbles in the slurry were discharged by vibrating for more than 2 min during each pouring;
(5) The samples were completely wrapped with plastic film and put into a standard curing box (temperature 20 ± 2 °C, humidity greater than 95%) for 1 day and then demolded, after which the samples were rewrapped and continuously cured until the set age.

2.3. Test Methods

For the sulfate attack test, the samples were fully immersed in 2.5% Na_2SO_4 and $MgSO_4$ solutions after 28 days of standard curing, as per the test method of Kamon et al. [31]. The immersion time was set to 3, 7, 28, 60, and 90 days. To eliminate testing errors in the samples, parallel samples were set to three for each immersion time. The sulfate solution was changed every 7 days. When the corresponding immersion age was reached, the samples were used for visual observation, UCS test, and mass change test.

The UCS test was carried out on a CMT5105 hydraulic servo universal testing machine, which was loaded by the displacement control method, and its loading rate was regulated to 1.0 mm/min. The representative core fragments of the samples after the UCS test were selected and put into an anhydrous ethanol of analytical purity level for 24 h to terminate the hydration reaction. Then, the fragments were dried at a low temperature

and analyzed for the phase composition (XRD test) and microstructural characteristics (SEM test). The XRD test procedure was performed by placing selected fragments in an agate bowl and manually grinding them through a 0.075 mm geotechnical sieve to make a powdered sample, which was carried out on an Ultima IV X-ray diffractometer with a step scan, a scan angle of 5°–90°, a scan speed of 8 °/min, and a step width of 0.02°. The SEM test procedure was performed by manually breaking the selected fragments into particles with a natural section and a size of about 5 mm, which were conducted on a ZEISS Gemini 300 backscattered scanning electron microscope with an accelerating voltage of 3 kV.

3. Results and Discussion

3.1. Visual Observation

The visual appearance of SF-GSSS immersed in a Na_2SO_4 solution for various time lengths is shown in Figure 2. It is shown that no significant physical deterioration of the surface of the SF-GSSS occurred when under the attack of a Na_2SO_4 solution. White precipitates appeared on the surface of S10F0 and interconnected microcracks appeared at its surrounding angles after 90 days of exposure to a Na_2SO_4 solution. A small amount of soil particles were found to fall off on the surface of S8F2, while the surface of S7F3 became rougher and showed a few pits due to the dislodging of soil particles in different ranges. It is noteworthy that the S9F1 surface was smooth and intact throughout the immersion cycle without significant deterioration. In agreement with the results of other studies in the literature [32,33], the SF-GSSS showed no significant surface deterioration under a long-term sodium sulfate attack, and it exhibited excellent resistance to sodium sulfate attack. Rashad et al. [34] indicated that a Na_2SO_4 solution with higher pH and more Na^+ capacity characteristics is more favorable for the inter-pore medium solution chemistry required for geopolymers to maintain performance stability. In addition to this, Bernal et al. [35] suggested that the attack of a Na_2SO_4 solution is committed to the further structural evolution and densification of the physical phase composition of the hydration products of geopolymers.

Figure 3 shows the visual appearance of SF-GSSS when immersed in a $MgSO_4$ solution for various time lengths. It is obvious that the surface deterioration of SF-GSSS presents different stage characteristics under a $MgSO_4$ attack condition. At the early stage of immersion, different degrees of white precipitates appeared on the surface of the samples, which can be attributed to the strong impermeability of the slag–fly-ash-based geopolymer stabilized soil. This resulted in the inability of the $MgSO_4$ solution to successfully immerse into the interior and to gather on the surface of the different samples. In the middle of the immersion period, swelling, peeling, and cracking were observed on the surface and around the corners of the different types of samples with large differences. At the later stage of immersion, the apparent structural integrity of the various samples was damaged to various degrees due to the continued development of cracks to interconnections and the shedding of soil particles over a large area. After 90 days of immersion in the $MgSO_4$ solution, the surface integrity of the samples were S9F1, S10F0, S8F2, and S7F3 in descending order. In line with the results of another study [36], the deterioration of geopolymer under the attack action of magnesium sulfate was more severe when compared to sodium sulfate.

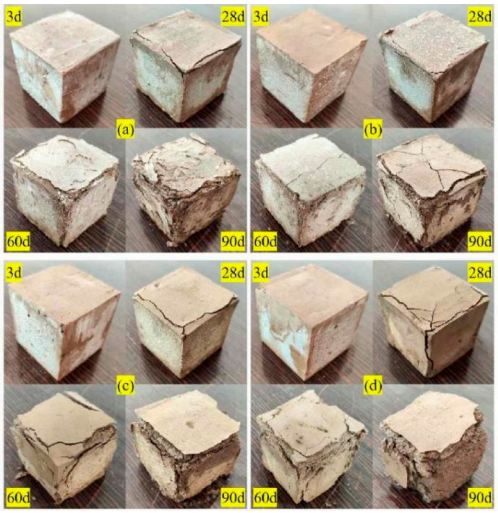

Figure 3. Visual appearance of SF-GSSS immersed in a $MgSO_4$ solution: (**a**) S10F0; (**b**) S9F1; (**c**) S8F2; and (**d**) S7F3.

3.2. Unconfined Compressive Strength

3.2.1. The UCS before Sulfate Attack

The UCS of the SF-GSSS before immersion in a sulfate solution is given in Figure 4. It is stated that the UCS of SF-GSSS exhibits a development trend that first starts with a small increase and then a larger decrease with the increase in fly ash admixture in the geopolymer precursor materials. The UCS of S10F0, S9F1, S8F2, and S7F3 were 7.405, 8.228, 5.760, and 4.525 MPa, respectively. With S10F0 as the control group, the strength growth rate of S9F1 was 11.1%, while the strength decrease rates of S8F2 and S7F3 were 22.2% and 38.9%, respectively. The growth of the strength of the samples by the appropriate amount of fly ash can be attributed to both the geopolymerization enhancement and lubrication effect. The specific significance of geopolymerization enhancement is that fly ash that is rich in silica-alumina mineral components can provide a large amount of reactive SiO_2, Al_2O_3, and Ca^{2+}. These compounds are provided by the slag undergoing a geopolymerization reaction under the catalytic effect of the composite alkali activator to produce more representative geopolymer gelling products, such as calcium silicate hydrate (C-S-H), the calcium silicate aluminate hydrate (C-A-S-H) of calcium-based hydration products, and the sodium-based hydration products consisting of sodium silicate aluminate hydrate (N-A-S-H). In addition, these products effectively improve the strength of the samples [37].

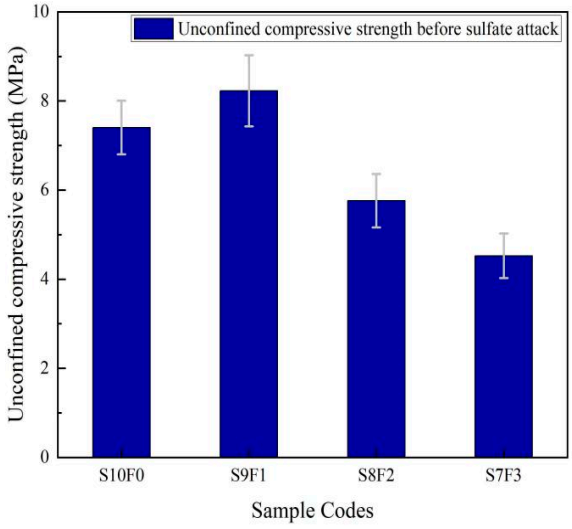

Figure 4. The UCS of SF-GSSS before sulfate attack.

The lubrication effect means that with the incorporation of spherical fly ash particles, the fluidity of the geopolymer slurry is greatly improved, which makes the slurry diffuse more uniformly in the soil, thus contributing to a denser and more stable microspatial structure of the sample. However, it is noteworthy that when the fly ash admixture exceeds a certain range, the geopolymer gel product (N-A-S-H) corresponding to the fly ash possesses the characteristics of a dense structure and strong chemical stability, which makes it difficult for the hydration reaction of the slag-based geopolymer hydration product to occur again. This results in a reduction in the hydration product and leads to a decrease in the cohesion of the soil particles [37]. The fly ash that did not participate in the geopolymerization reaction is only present in the specimen as a mineral admixture in the form of physical filling, which increases the porosity and has a side effect on the strength [30].

3.2.2. The UCS after Immersion in Na_2SO_4 Solution

Figure 5 shows the UCS of the SF-GSSS after immersion in a Na_2SO_4 solution at different times. The UCS of the SF-GSSS with different slag/fly ash ratios all exhibited a gradual decreasing trend with the extension of the immersion period. At the early stage of immersion (7 days of immersion), the strength of S10F0, S9F1, S8F2, and S7F3 were 7.000, 7.850, 5.382, and 4.186 MPa, with strength change rates of −5.47%, −4.59%, −6.56%, and −7.49%, respectively. It can be seen that the SF-GSSS is more impermeable and structurally stable at the early stage of immersion, which makes it impossible for the Na_2SO_4 solution to easily invade into the internal structure of the specimen with less strength loss. When the exposure to a Na_2SO_4 solution was extended to 90 days, the strength of S10F0, S9F1, S8F2, and S7F3 decreased to 6.035, 7.127, 4.806, and 3.591 MPa, with strength change rates of −18.50%, −13.38%, −16.56%, and −20.64%, respectively. Bakharev et al. [36] stated that the most important reason for the loss of mechanical properties of geopolymers immersed in a Na_2SO_4 solution is the generation of microcracks inside the specimen. The microcracks can be explained by the mutual exchange in Ca^{2+} and Na^+ in a Na_2SO_4 solution, which causes stress inside the specimen. The ion exchange rate is determined by the permeability performance of the specimen, which mainly consists of the pore structure and pore size [38]. This matches with the experimental results, where it was observed that the resistance of the SF-GSSS to attack by a Na_2SO_4 solution showed a development trend of increasing and then decreasing with the increase in fly ash admixture in the precursor materials, which is mainly related to the pore structure characteristics of the specimen.

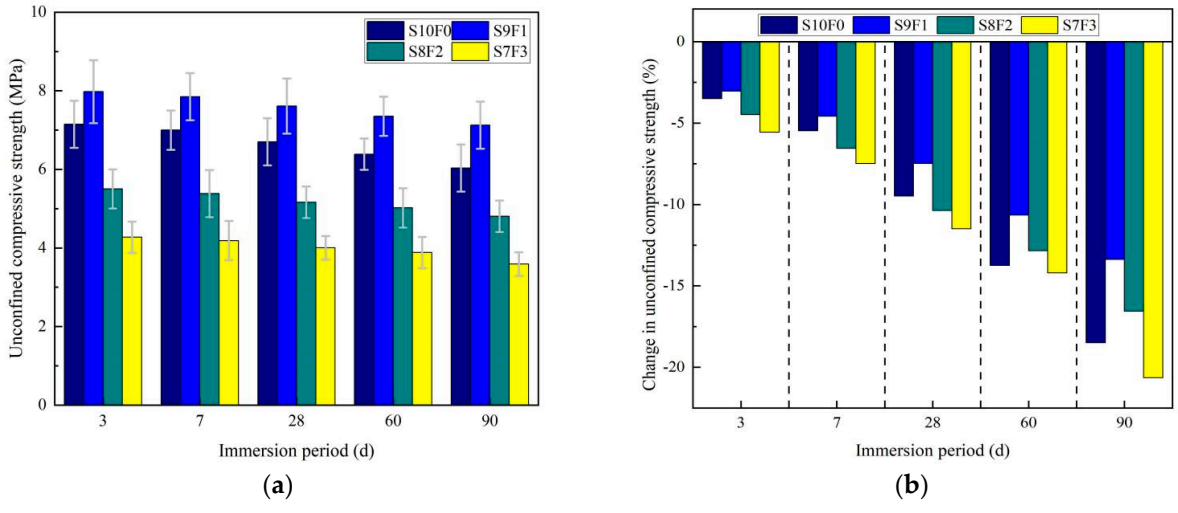

(**a**) (**b**)

Figure 5. (**a**) The UCS of SF-GSSS immersed in Na_2SO_4 solution at different times. (**b**) Change in UCS.

3.2.3. The UCS after Immersion in $MgSO_4$ Solution

The UCS of SF-GSSS after immersion in a $MgSO_4$ solution at various times is given in Figure 6. The UCS of the samples showed segmented regional characteristics with the extension of the immersion period. The strength decreased relatively slowly until 28 days of immersion, while the strength of the samples exhibited a significant decrease when the age of immersion exceeded 28 days. When exposed to a $MgSO_4$ solution for 90 days, the strengths of S10F0, S9F1, S8F2, and S7F3 decreased to 4.024, 5.550, 2.272, and 0.667 MPa, with strength decreases of 45.66%, 32.55%, 60.55%, and 85.26%, respectively. The above results state that the degradation effect of a $MgSO_4$ solution on SF-GSSS is much greater than that of a Na_2SO_4 solution.

This result is consistent with other studies [39,40] which reported that the slag–fly-ash-based geopolymer exhibited a severe deterioration of its apparent and mechanical properties under the attack of a $MgSO_4$ solution, while the less damage was suffered in a Na_2SO_4 solution. Ye et al. [41] and Bonen et al. [42] suggested that under the attack of $MgSO_4$, the geopolymer gel products undergo degradation phenomena such as strong decalcification and silicate polymerization, resulting in the transformation of C-A-S-H and N-A-S-H with high cementation capacity to M-A-S-H with low mechanical properties and poor cementation capacity. In addition, the expansion stresses caused by the chemical reaction between Ca^{2+} separate after the decalcification of aluminosilicate and $SO4^{2-}$ in a sulfate solution, which generate an expansion product such as gypsum, and which directly or indirectly lead to deterioration, such as the cracking and peeling of the samples [43]. The above degradation phenomenon is in agreement with the apparent changes in samples immersed in a $MgSO_4$ solution, where the apparent integrity of different types of samples suffered different degrees of damage due to the effects of swelling and cracking. Compared to S10F0 and S9F1, the more serious strength loss of S8F2 and S7F3 may be due to the greater porosity of the specimen, which makes it easier for the $MgSO_4$ solution to soak into the interior of the specimen.

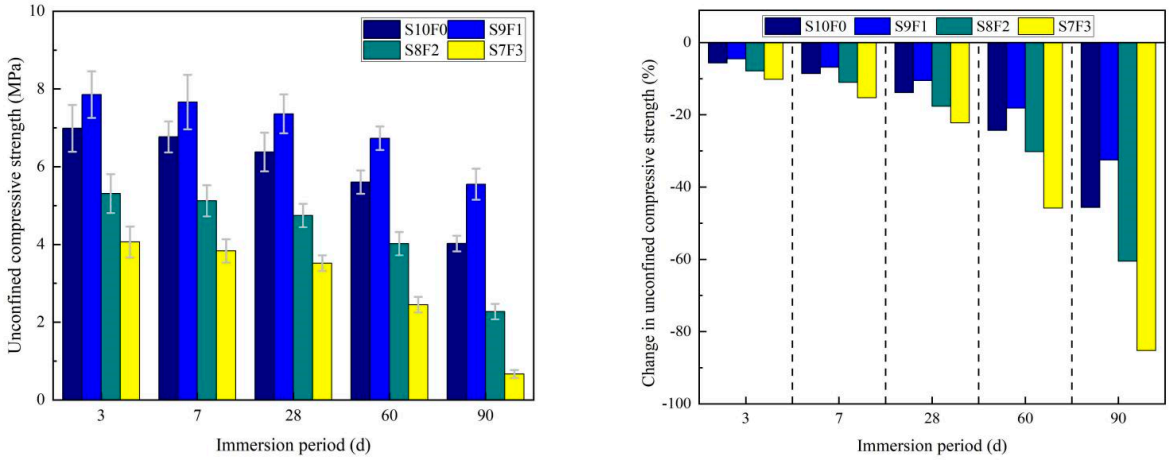

(**a**) (**b**)

Figure 6. (**a**) The UCS of SF-GSSS immersed in $MgSO_4$ solution at various times. (**b**) Change in UCS.

3.3. Mass Change

Figure 7 shows the trend of the mass change in SF-GSSS when immersed in a Na_2SO_4 or $MgSO_4$ solution. It is obvious that the type of sulfate solution has a non-negligible effect on the mass change in the samples. Whether immersed in a Na_2SO_4 or $MgSO_4$ solution, the mass of the samples showed a gradual increase with the growth of the immersion period, but the increase in the mass of the SF-GSSS immersed in a $MgSO_4$ solution was much larger than when it was immersed in a Na_2SO_4 solution. When exposed to a Na_2SO_4 solution for 90 days, the mass change rates of S10F0, S9F1, S8F2, and S7F3 were 1.38%, 1.18%, 1.30%, and 1.46%, respectively. The variation in mass of the SF-GSSS was not significant. It is not

difficult to infer that the mass of the SF-GSSS immersed in a Na_2SO_4 solution is stable and has good resistance to Na_2SO_4 attack without significant structural changes. The above results can be explained by the fact that the change in mass of the samples immersed in a Na_2SO_4 solution depends mainly on the pore structure characteristics.

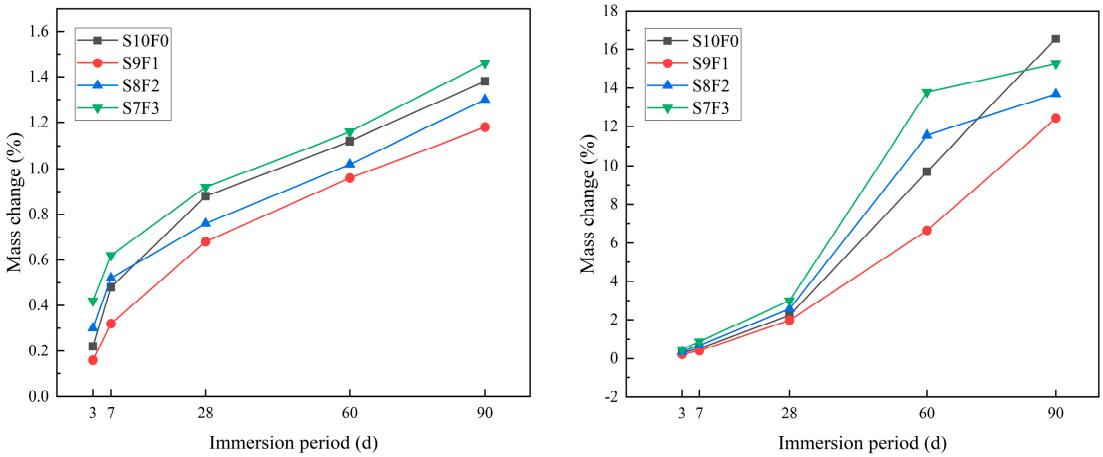

Figure 7. Mass change in SF-GSSS at different immersion periods: (**a**) Na_2SO_4 solution and (**b**) $MgSO_4$ solution.

In the attack environment of a $MgSO_4$ solution, with the immersion age of 28 days as the cut-off point, the mass of the samples first increased slowly and then increased substantially. The above mass change trend can be explained by the chemical reaction between the decalcification and dealumination of C(N)-A-S-H and $MgSO_4$ to produce expansive substances such as gypsum, resulting in the destruction of the sample pore structure and an increase in porosity, thus leading to a further intrusion of the $MgSO_4$ solution into the sample and the generation of more gypsum [43]. The mass change rates of S10F0, S9F1, S8F2, and S7F3 were 16.55%, 12.43%, 13.68%, and 15.25% at 90 days of immersion, respectively. The decrease in the mass growth rate of S8F2 and S7F3 when compared to S10F0 and S9F1 may be due to the fact that the expansion stress of the gypsum was greater than the maximum load-bearing capacity of the specimen pore wall, resulting in different degrees of surface shedding [40]. This is in agreement with the apparent change in the samples.

3.4. XRD Analysis

The XRD patterns of the SF-GSSS before a sulfate solution attack are given in Figure 8. The SF-GSSS with different slag/fly ash ratios are composed of a large number of crystalline and amorphous phase products. The mineral components of S10F0 consist mainly of quartz, calcite, and calcium-based hydration products such as C-S-H and C-A-S-H. This is in agreement with the findings reported in the literature [18,37], where C-S-H and C-A-S-H allowed an effective development of the early strength of the samples. Quartz may be derived from soft soil and precursors, which are not involved in the hydration of geopolymer, while calcite formation may be due to the carbonation of the sample during curing. The sodium-based hydration product (N-A-S-H) was obtained in S9F1, which explains the effective improvement of the strength of S9F1 when compared to S10F0. The intensity of the diffraction peaks of C-S-H and C-A-S-H in S8F2 and S7F3 gradually decreased with the increase in fly ash admixture in the precursor materials, which can be explained by the difficulty of the chemical reaction between the N-A-S-H with a dense structure and strong chemical stability and the slag-based geopolymer gel products, which inhibited the development of a slag hydration reaction [30,37].

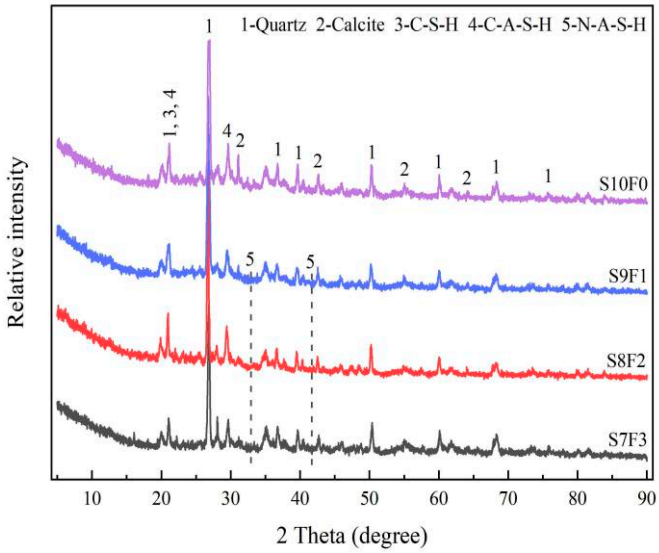

Figure 8. XRD analysis of SF-GSSS before sulfate attack.

Figure 9 shows the XRD patterns of the SF-GSSS exposed to Na_2SO_4 or $MgSO_4$ solutions for 60 days, respectively. Figure 9a demonstrates that the mineral phases of the samples did not change significantly after the attack of the Na_2SO_4 solution. This is in accordance with the study of Zhang et al. [43], where trace amounts of ettringite were found in S10F0, which was mainly attributed to the slight decalcification and dealumination of the calcium-rich silicate gel by Na_2SO_4 attack. The mineral phases of S9F1 and S8F2 were identical to those before immersion, and no ettringite was generated, which can prove that the blending of the appropriate amount of fly ash can improve the resistance of the samples to Na_2SO_4 attack. The above phenomenon may be related to the structural stability of N-A-S-H and the decrease in the Ca/Si ratio in C-A-S-H [44]. However, the presence of ettringite in S7F3 suggests that the excessive fly ash admixture has a detrimental effect on the resistance of the samples to Na_2SO_4 attack. It can be explained that the higher porosity of S7F3 makes it easy for the Na_2SO_4 solution to penetrate into the sample, which accelerates the decalcification and dealumination process of C-A-S-H.

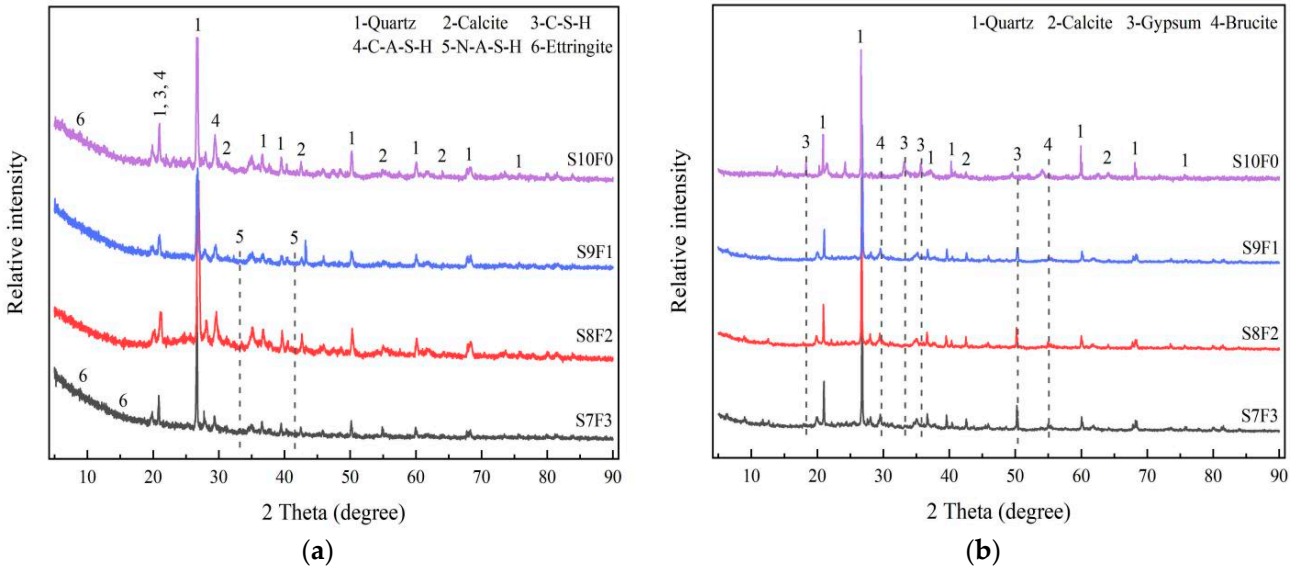

Figure 9. XRD analysis of SF-GSSS after 60 days immersion: (**a**) Na_2SO_4 solution and (**b**) $MgSO_4$ solution.

Figure 9b shows an obvious change in the mineral phase of the SF-GSSS under the attack of $MgSO_4$, which is mainly reflected by the disappearance of representative gelling substances such as the C-S-H, C-A-S-H, and N-A-S-H diffraction peaks, and the appearance of gypsum and brucite characteristic peaks. Certain studies in the literature [39,45] reported that the deterioration mechanism of $MgSO_4$ on geopolymer materials, prepared from slag and fly ash, is mainly to convert C-S-H, C-A-S-H, and N-A-S-H to poorly cemented M-S-H and M-A-S-H. However, no M-S-H and M-A-S-H diffraction peaks were found in the samples, which is in accordance with the reported results [43]. Compared with S10F0, the diffraction peak intensity of gypsum in S9F1 and S8F2 gradually decreased, which can be attributed to the increase in N-A-S-H production with high chemical stability; in addition, the decrease in Ca content in the geopolymer stabilized soil system occurred as the amount of fly ash admixture in the precursor material increased [46]. The high intensity of the gypsum characteristic peak in S7F3 may be due to the high porosity that accelerates the efficiency of the $MgSO_4$ solution to leach into the internal structure of the specimen [43]. The lower activity originating from fly ash requires more OH^- to be activated, which attenuates the effective OH^- in the geopolymer stabilized soil system [37]. Therefore, the intensity of the diffraction peak of brucite gradually decreases with the progressive fly ash admixture. Moreover, the reason for not generating ettringite after the attack of $MgSO_4$ is that the pH of $MgSO_4$ solution is obviously lower than that of the Na_2SO_4 solution under the same conditions of immersion age, as well as ettringite not being stable within the environment of lower pH [47].

3.5. SEM Analysis

Figure 10 shows the SEM images of the SF-GSSS before sulfate attack. The plate-like gelling substances were found in S10F0, which completely encapsulated soil particles and filled the excess pores of the internal structure of the soil to form stable soil agglomerates, resulting in enhanced internal structural compactness. The rest of the gels were interconnected after solidification and hardened to form a geopolymer stabilized soil space structure system [48]. The two together effectively improved the mechanical properties of the soil. It is important to note that there were a few microporous defects in S10F0, which were mainly due to the geopolymer slurry setting and hardening too fast during the mixing process, and due to its poor fluidity making it difficult to make full contact with the soil. With the incorporation of fly ash, flocculent gelling substances were found in S9F1, and the structural denseness of the specimen was further enhanced with an intact surface. Few fly ash particles and slag particles were found around the gelling substances in S8F2 and S7F3, which are mainly fly ash with lower activity and dense structures, resulting in them consuming more of the alkali activator [49]. Moreover, the N-A-S-H structure makes it difficult to react again with the hydration of the slag-based geopolymer gel products [37]. Fly ash and slag particles that did not participate in the geopolymerization reaction were present in the soil in a physically filled manner, increasing the porosity of the specimen. Compared with S8F2, the microstructure of S7F3 was sparser and more porous, and the integrity was reduced.

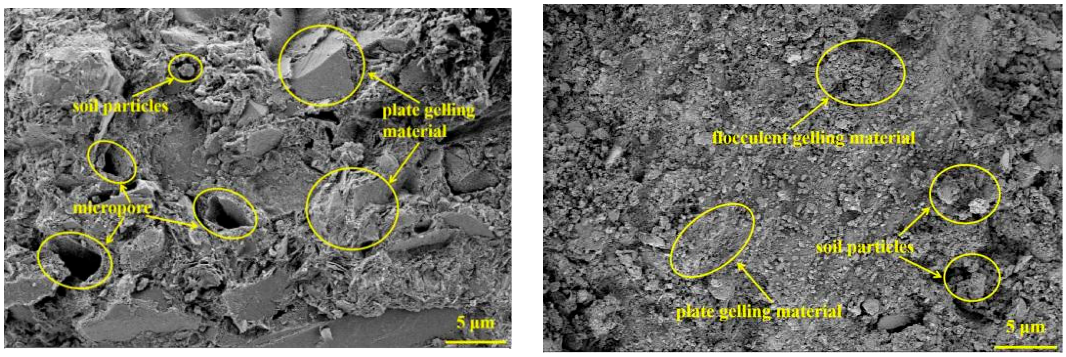

(**a**) (**b**)

Figure 10. *Cont.*

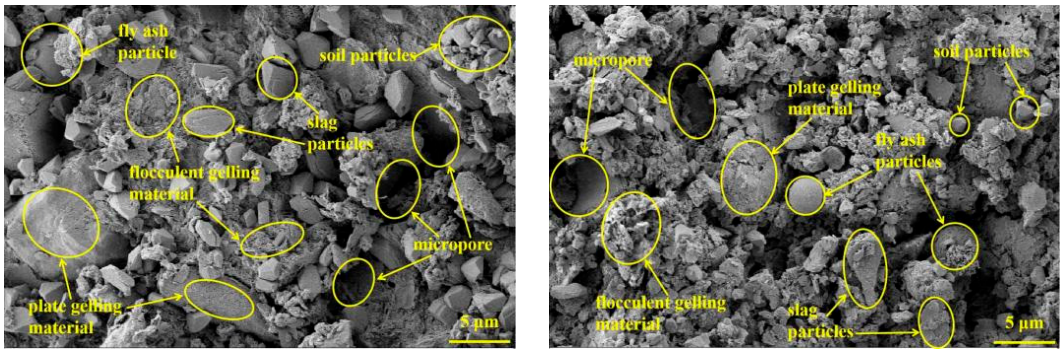

(**c**) (**d**)

Figure 10. SEM analysis of SF-GSSS before sulfate attack: (**a**) S10F0; (**b**) S9F1; (**c**) S8F2; and (**d**) S7F3.

Figure 11 shows the SEM images of SF-GSSS after 60 days of immersion in a Na_2SO_4 solution. A few sporadically distributed micropores, microcracks, and needle-rod ettringite were found in S10F0, where the ettringite mainly occurred via the decalcification and dealumination of the calcium-rich cementation products caused by the attack of the Na_2SO_4 solution [38]. It can be speculated that the generation of trace cracks on the surface of S10F0 can be partly attributed to the expansion stress of ettringite. Microcracks were also found in S9F1 and S8F2, which confirmed that the generation of microcracks was the main reason for the damage of the SF-GSSS in a Na_2SO_4 attack environment. A large amount of ettringite was found in S7F3, which led to a change in the internal structural configuration of the specimen to be loose and porous. Although the surface of S7F3 was relatively well integrated at the end of the attack, more microcracks may have been generated in its internal structure, which explains the faster decrease in the strength of the sample at the late immersion stage.

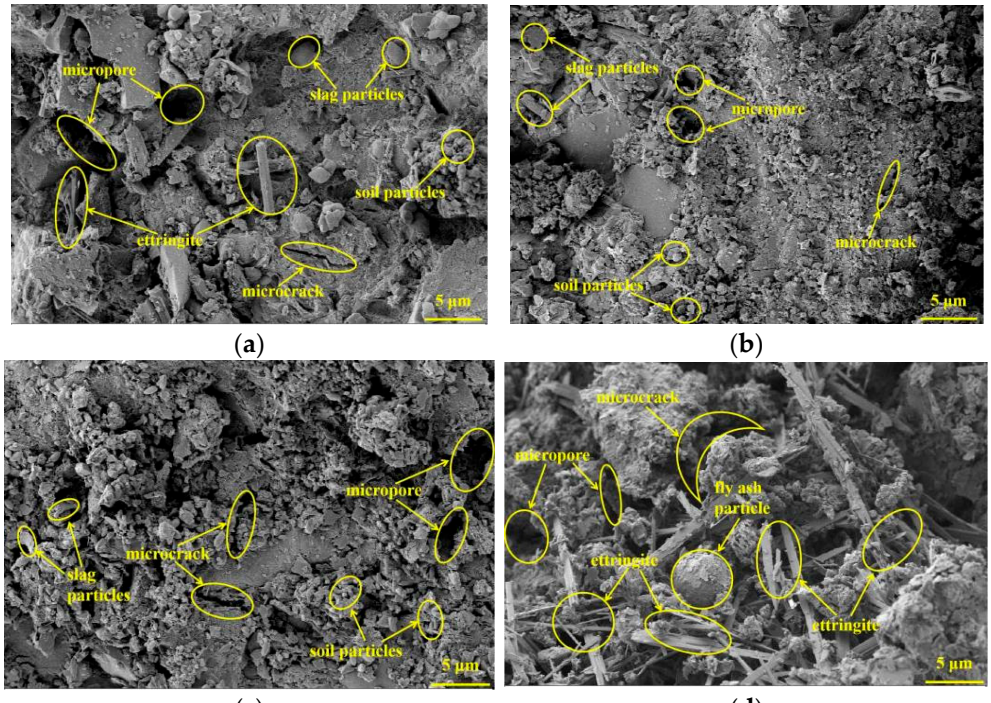

(**a**) (**b**)

(**c**) (**d**)

Figure 11. SEM analysis of SF-GSSS immersed in a Na_2SO_4 solution for 60 days: (**a**) S10F0; (**b**) S9F1; (**c**) S8F2; and (**d**) S7F3.

The SEM images of SF-GSSS after 60 days of exposure to a $MgSO_4$ solution are given in Figure 12. Obviously, gypsum was found in S10F0, S9F1, S8F2, and S7F3 with different distribution ranges. It can be inferred that gypsum is the main substance produced after the attack of SF-GSSS by a $MgSO_4$ solution. With the continuous accumulation of gypsum, the generated expansion stress grew gradually until it was larger than the maximum load-bearing capacity of the pore wall, which lead to different degrees of damage to the microstructure of the samples. A relatively high number of hole defects were found in S10F0. The gelling substances inside S9F1 and S8F2 were significantly reduced, and their cementitious properties to soil particles became poor, making the overall structure loose and porous with a sheet-like stack. In particular, more cracks were generated in S8F2. The decrease in cementation property was mainly due to the conversion of C-S-H, C-A-S-H, and N-A-S-H to M-S-H and M-A-S-H after the replacement of alkali metal cations by Mg^{2+}, which has poorer mechanical properties and weaker cementation [36]. A large amount of disordered gypsum was found in S7F3, and the internal structure of the specimen had completely lost its integrity and transformed into a hollow structure.

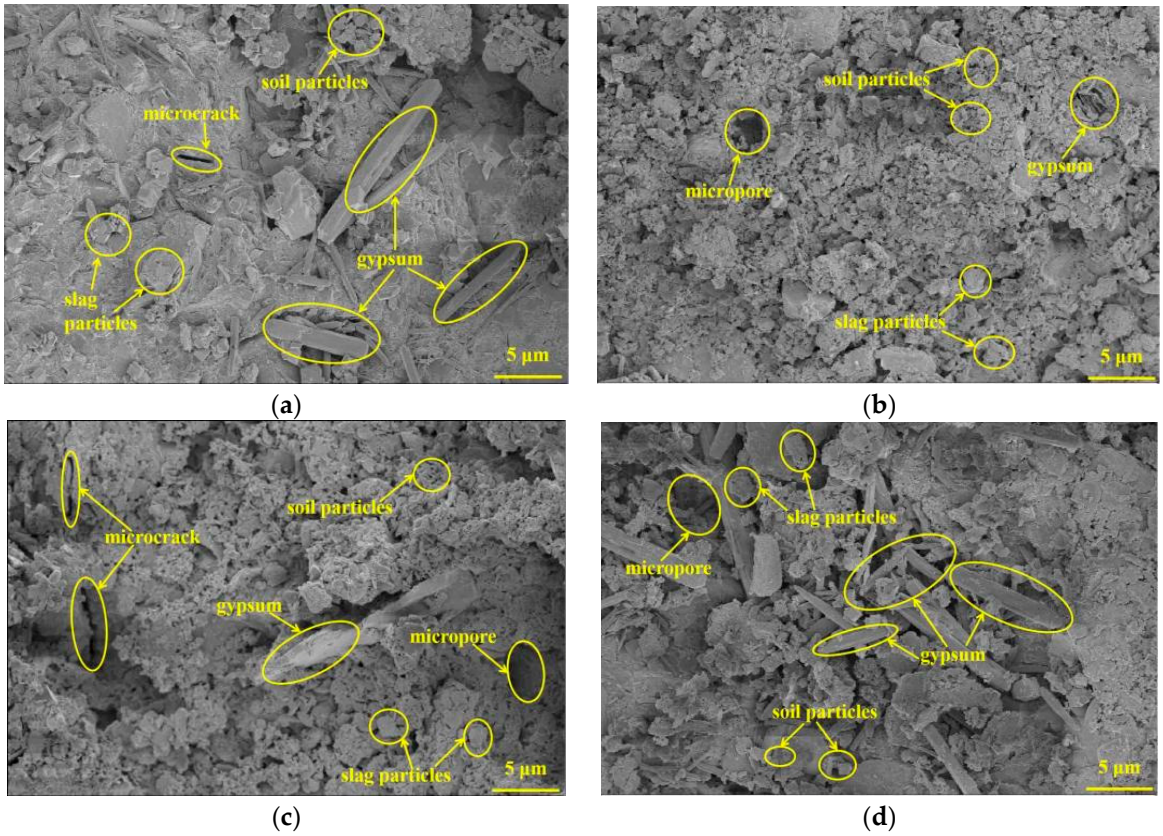

Figure 12. SEM analysis of SF-GSSS immersed in $MgSO_4$ solution for 60 days: (**a**) S10F0; (**b**) S9F1; (**c**) S8F2; and (**d**) S7F3.

4. Mechanism Analysis of Sulfate Attack

The deterioration mechanism of the Na_2SO_4 solution on the performance of slag–fly-ash-based geopolymer stabilized soft soil was mainly reflected in the formation of microcracks and due to the expansion and cracking of ettringite. The generation of microcracks originated from stresses generated by the exchange in the alkali metal cations of aluminosilicate gel products with Na^+ in a Na_2SO_4 solution [36]. The ion exchange rate depends on the pore structure characteristics of the sample, which is proportional to the porosity [38]. It can be seen from the SEM images that microcracks with different distribution ranges were found in S10F0, S9F1, S8F2, and S7F3, and the number of microcracks showed a development trend of first decreasing and then increasing with the increase

in fly ash content. The above results can be explained by the fact that the incorporation of fly ash changed the pore structure of the samples. The additional hydration products and lubricating effect provided by incorporating the appropriate amount of fly ash can effectively improve the compactness of the samples [37]. However, excessive incorporation of fly ash is counterproductive, mainly because the structurally stable N-A-S-H hinders the development process of the hydration reaction of slag and reduces the generation of hydration products, as well as because fly ash that is partially filled in a physical way without participating in the hydration reaction increases the porosity of the samples [30].

On the other hand, the formation of ettringite is mainly due to the chemical reaction between C-A-S-H, which undergoes decalcification and dealumination, and SO_4^{2-} in a sulfate solution [43]. Traces of ettringite were found in S10F0 and S7F3, which suggested that the production of ettringite may be related to the calcium content and porosity of the samples. In contrast, no ettringite was found in S9F1 and S8F2, indicating that a moderate amount of fly ash can inhibit the formation of ettringite, which can be attributed to the structural stability of N-A-S-H and due to the decrease in the Ca/Si ratio in C-A-S-H [44]. Although S10F0 and S7F3 showed a few microcracks and soil particles falling off at the end of the immersion period, the surface was still relatively intact, which indicates that the expansion of ettringite was not significant. In summary, it was shown that the attack effect of the Na_2SO_4 solution on the samples was dominated by the formation of microcracks and was supplemented by the expansion cracking of ettringite.

The deterioration mechanism of the $MgSO_4$ solution on the performance of the slag–fly-ash-based geopolymer stabilized soft soil was mainly composed of a weak cementation effect and the expansion and cracking of gypsum. The weak cementation effect refers to the transformation of C-S-H, C-A-S-H, and N-A-S-H into M-S-H and M-A-S-H with poor mechanical properties and weak cementation ability under the replacement effect of Mg^{2+} [41,42]. The above results make the gel substance less adhesive to soil particles, causing the disintegration of soil particle agglomerates and leading to deterioration phenomena such as soil particles falling off, as well as peeling on the surface of the samples. From the apparent changes, it can be seen that S10F0, S8F2, and S7F3 showed different degrees of soil particles shedding at the end of immersion, while S9F1 was relatively intact, which was mainly due to the structurally stable, and with a high chemical stability, N-A-S-H [46].

In addition, the replaced Ca^{2+} reacted chemically with SO_4^{2-} to produce gypsum with expansion characteristics, which damaged the microstructure and lead to deterioration characteristics such as the expansion and cracking of the samples [43]. Within a certain range, the incorporation of fly ash can effectively inhibit the formation of gypsum because of the high chemical stability of N-A-S-H and due to the reduction in Ca content in the geopolymer stabilized soil system [46]. However, mixing too much fly ash can be counterproductive, which can be explained by the increase in the porosity of the samples, which accelerated the attack efficiency of the $MgSO_4$ solution [30].

In summary, it can be seen that the attack of sulfate is closely related to alkali metal cations, of which Mg^{2+} possesses a more prominent erosive property than Na^+. Compared to Na_2SO_4, $MgSO_4$ is not only a type of SO_4^{2-} attack, Mg^{2+} also has the effect of displacing the cations of gelling products, thus weakening the adhesive effect of the gel [39,45]. On the other hand, the variability in the erosivity of different sulfates may also be linked to the ability to change the pH of the pore solution. Zhang et al. [43] found that the pH of the solution after a $MgSO_4$ attack was lower than that of Na_2SO_4 at the same immersion age, which was not conducive to the structural evolution and crystalline phase densification of geopolymer hydration products [35].

5. Conclusions

The purpose of this study was to elucidate the effect of Na_2SO_4 and $MgSO_4$ solutions on the durability of SF-GSSS with different slag/fly ash ratios, as well as to characterize the deterioration mechanisms of the Na_2SO_4 and $MgSO_4$ solutions on the samples via visual observations, UCS tests, mass changes, and through microscopic testing means such as

SEM and XRD analysis. Considering the experimental results of the study, the conclusions obtained are shown below:

(1) The surface of SF-GSSS attacked by a Na_2SO_4 solution showed no obvious deterioration, while the surface of SF-GSSS attacked by a $MgSO_4$ solution showed serious physical deterioration, such as swelling, cracking, and the shedding of soil particles;
(2) The mass of SF-GSSS increased with the extension of the immersion period, whether immersed in a Na_2SO_4 or $MgSO_4$ solution. At the same immersion age, the degree of mass growth of SF-GSSS immersed in a Na_2SO_4 solution was much lower than that of SF-GSSS immersed in a $MgSO_4$ solution;
(3) The UCS of SF-GSSS immersed in a Na_2SO_4 solution gradually decreased during the immersion period, while the UCS of SF-GSSS under the attack effect of a $MgSO_4$ solution gradually decreased until 28 days of the immersion age, after which a significant decrease in strength occurred. In addition, the strength loss rate, throughout the immersion cycle, of SF-GSSS immersed in a $MgSO_4$ solution was greater than when it was immersed in a Na_2SO_4 solution;
(4) There is an important relationship between the slag/fly ash ratio and the resistance of SF-GSSS to sulfate attack. When exposed to Na_2SO_4 and $MgSO_4$ solutions for 90 days, the strength loss rate of S9F1 was the lowest, which were 13.38% and 20.64%, and the strength loss rate of S7F3 was the highest, which were 20.64% and 85.26%, respectively;
(5) The results of the XRD and SEM analysis indicated that the attack deterioration of the Na_2SO_4 solution mainly included the formation of microcracks and the expansion and cracking action of ettringite, while the $MgSO_4$ solution mainly consisted of a weak cementation effect, as well as the swelling and cracking action of gypsum.

Author Contributions: Conceptualization, X.Y., B.Z. and G.Z.; investigation, G.W., Y.L. and Z.L.; writing—original draft preparation, G.W., Y.L. and Z.L.; writing—review and editing, X.Y., B.Z. and G.Z. All authors have read and agreed to the published version of the manuscript.

Funding: This work was financially supported by the Open Research Fund of the Key Laboratory of Construction and Safety of Water Engineering of the Ministry of Water Resources, China Institute of Water Resources and Hydropower Research (no. 202109); the Education Department Research Foundation of Hunan Province (nos. 21B0123 and 21A0511); and the Postgraduate Scientific Research Innovation Project of Hunan Province (no. QL20210155).

Data Availability Statement: The data used to support the results of this study are available from the corresponding author upon reasonable request.

Conflicts of Interest: The authors declare that they have no known competing financial interest or personal relationship that could have appeared to influence the work reported in this paper.

References

1. Cristelo, N.; Glendinning, S.; Fernandes, L.; Pinto, A.T. Effects of alkaline-activated fly ash and Portland cement on soft soil stabilisation. *Acta Geotech.* **2013**, *8*, 395–405. [CrossRef]
2. Chompoorat, T.; Thepumong, T.; Khamplod, A.; Likitlersuang, S. Improving mechanical properties and shrinkage cracking characteristics of soft clay in deep soil mixing. *Constr. Build. Mater.* **2022**, *316*, 125858. [CrossRef]
3. Zhang, G.; Ding, Z.; Wang, Y.; Fu, G.; Wang, Y.; Xie, C.; Zhang, Y.; Zhao, X.; Lu, X.; Wang, X. Performance Prediction of Cement Stabilized Soil Incorporating Solid Waste and Propylene Fiber. *Materials* **2022**, *15*, 4250. [CrossRef] [PubMed]
4. Firoozi, A.A.; Guney Olgun, C.; Firoozi, A.A.; Baghini, M.S. Fundamentals of soil stabilization. *Int. J. Geo-Eng.* **2017**, *8*, 26. [CrossRef]
5. Zhang, G.; Ding, Z.; Zhang, R.; Chen, C.; Fu, G.; Luo, X.; Wang, Y.; Zhang, C. Combined utilization of construction and demolition waste and propylene fiber in cement-stabilized soil. *Buildings* **2022**, *12*, 350. [CrossRef]
6. Luo, Z.; Zhang, B.; Zou, J.; Luo, B. Sulfate erosion resistance of slag-fly ash based geopolymer stabilized soft soil under semi-immersion condition. *Case Stud. Constr. Mat.* **2022**, *17*, e01506. [CrossRef]
7. Maddalena, R.; Roberts, J.J.; Hamilton, A. Can Portland cement be replaced by low-carbon alternative materials? A study on the thermal properties and carbon emissions of innovative cements. *J. Clean. Prod.* **2018**, *186*, 933–942. [CrossRef]
8. Davidovits, J. Geopolymers: Inorganic polymeric new materials. *J. Therm. Anal. Calorim.* **1991**, *37*, 1633–1656. [CrossRef]

9. Qaidi, S.M.A.; Tayeh, B.A.; Ahmed, H.U.; Emad, W. A review of the sustainable utilisation of red mud and fly ash for the production of geopolymer composites. *Constr. Build. Mater.* **2022**, *350*, 128892. [CrossRef]
10. Ozturk, M.; Arslan, G. Shear Behavior of Granulated Blast Furnace Slag-Based Geopolymer-Reinforced Concrete Beams. *Buildings* **2022**, *12*, 2053. [CrossRef]
11. Sruthi, S.; Gayathri, V. Synthesis and Evaluation of Eco-Friendly, Ambient-Cured, Geopolymer-Based Bricks Using Industrial By-Products. *Buildings* **2023**, *13*, 510. [CrossRef]
12. Singh, N.B.; Middendorf, B. Geopolymers as an alternative to Portland cement: An overview. *Constr. Build. Mater.* **2020**, *237*, 117455. [CrossRef]
13. Amer, A.A.; El-Hoseny, S. Properties and performance of metakaolin pozzolanic cement pastes. *J. Therm. Anal. Calorim.* **2017**, *129*, 33–44. [CrossRef]
14. Tan, J.; Cai, J.; Huang, L.; Yang, Q.; Mao, M.; Li, J. Feasibility of using microwave curing to enhance the compressive strength of mixed recycled aggregate powder based geopolymer. *Constr. Build. Mater.* **2020**, *262*, 120897. [CrossRef]
15. Sahoo, S.; Singh, S.P. Strength and durability properties of expansive soil treated with geopolymer and conventional stabilizers. *Constr. Build. Mater.* **2022**, *328*, 127078. [CrossRef]
16. Ghadir, P.; Zamanian, M.; Mahbubi-Motlagh, N.; Saberian, M.; Li, J.; Ranjbar, N. Shear strength and life cycle assessment of volcanic ash-based geopolymer and cement stabilized soil: A comparative study. *Transp. Geotech.* **2021**, *31*, 100639. [CrossRef]
17. Zhou, H.; Wang, X.; Wu, Y.; Zhang, X. Mechanical properties and micro-mechanisms of marine soft soil stabilized by different calcium content precursors based geopolymers. *Constr. Build. Mater.* **2021**, *305*, 124722. [CrossRef]
18. Samantasinghar, S.; Singh, S.P. Strength and Durability of Granular Soil Stabilized with FA-GGBS Geopolymer. *J. Mater. Civil. Eng.* **2021**, *33*, 06021003. [CrossRef]
19. Bilondi, M.P.; Toufigh, M.M.; Toufigh, V. Experimental investigation of using a recycled glass powder-based geopolymer to improve the mechanical behavior of clay soils. *Constr. Build. Mater.* **2018**, *170*, 302–313. [CrossRef]
20. Luo, Y.; Meng, J.; Wang, D.; Jiao, L.; Xue, G. Experimental study on mechanical properties and microstructure of metakaolin based geopolymer stabilized silty clay. *Constr. Build. Mater.* **2022**, *316*, 125662. [CrossRef]
21. Rollings, R.S.; Burkes, J.P.; Rollings, M.P. Sulfate attack on cement-stabilized sand. *J. Geotech. Geoenviron.* **1999**, *125*, 364–372. [CrossRef]
22. Rajasekaran, G. Sulphate attack and ettringite formation in the lime and cement stabilized marine clays. *Ocean Eng.* **2005**, *32*, 1133–1159. [CrossRef]
23. Puppala, A.J.; Intharasombat, N.; Vempati, R.K. Experimental studies on ettringite-induced heaving in soils. *J. Geotech. Geoenviron.* **2005**, *131*, 325–337. [CrossRef]
24. Han, P.; Wang, S.; Chen, F.Y.; Bai, X. Mechanism of cement-stabilized soil polluted by magnesium sulfate. *J. Cent. South Univ.* **2015**, *22*, 1869–1877. [CrossRef]
25. Bonen, D.; Cohen, M.D. Magnesium sulfate attack on portland cement paste-I. Microstructural analysis. *Cem. Concr. Res.* **1992**, *22*, 169–180. [CrossRef]
26. Singh, B.; Ishwarya, G.; Gupta, M.; Bhattacharyya, S.K. Geopolymer concrete: A review of some recent developments. *Constr. Build. Mater.* **2015**, *85*, 78–90. [CrossRef]
27. Vikas, G.; Rao, T.D. Setting time, workability and strength properties of alkali activated fly Ash and slag based geopolymer concrete activated with high silica modulus water glass. *IJST-Trans. Civ. Eng.* **2021**, *45*, 1483–1492. [CrossRef]
28. Wang, S.D.; Scrivener, K.L.; Pratt, P.L. Factors affecting the strength of alkali-activated slag. *Cem. Concr. Res.* **1994**, *24*, 1033–1043. [CrossRef]
29. Chew, S.H.; Kamruzzaman, A.H.M.; Lee, F.H. Physicochemical and engineering behavior of cement treated clays. *J. Geotech. Geoenviron.* **2004**, *130*, 696–706. [CrossRef]
30. Luo, Z.; Luo, B.; Zhao, Y.; Li, X.; Su, Y.; Huang, H.; Wang, Q. Experimental Investigation of Unconfined Compression Strength and Microstructure Characteristics of Slag and Fly Ash-Based Geopolymer Stabilized Riverside Soft Soil. *Buildings* **2022**, *14*, 307. [CrossRef] [PubMed]
31. Kamon, M.; Nontananandh, S.; Katsumi, T. Utilization of stainless-steel slag by cement hardening. *Soils Found.* **1993**, *33*, 118–129. [CrossRef] [PubMed]
32. Sukmak, P.; Silva, P.D.; Horpibulsuk, S.; Chindaprasirt, P. Sulfate resistance of clay-portland cement and clay high-calcium fly ash geopolymer. *J. Mater. Civil. Eng.* **2015**, *27*, 04014158. [CrossRef]
33. Jiang, N.J.; Du, Y.J.; Liu, K. Durability of lightweight alkali-activated ground granulated blast furnace slag (GGBS) stabilized clayey soils subjected to sulfate attack. *Appl. Clay Sci.* **2018**, *161*, 70–75. [CrossRef]
34. Rashad, A.M.; Bai, Y.; Basheer, P.A.M.; Collier, N.C.; Milestone, N.B. Chemical and mechanical stability of sodium sulfate activated slag after exposure to elevated temperature. *Cem. Concr. Res.* **2012**, *42*, 333–343. [CrossRef]
35. Bernal, S.A.; Provis, J.L. Durability of alkali-activated materials: Progress and perspectives. *J. Am. Ceram. Soc.* **2014**, *97*, 997–1008. [CrossRef]
36. Bakharev, T. Durability of geopolymer materials in sodium and magnesium sulfate solutions. *Cem. Concr. Res.* **2005**, *35*, 1233–1246. [CrossRef]
37. Wu, J.; Zheng, X.; Yang, A.; Li, Y. Experimental study on compressive strength of slag-fly ash based geopolymer stabilized silty clay. *Rock Soil Mech.* **2021**, *42*, 647–655. (In Chinese)

38. Park, K.S.; Ni, Z.; Côté, A.P.; Yaghi, O.M. Exceptional chemical and thermal stability of zeolitic imidazolate frameworks. *Proc. Natl. Acad. Sci. USA* **2006**, *103*, 10186–10191. [CrossRef]
39. Ismail, I.; Bernal, S.A.; Provis, J.L.; Hamdan, S.; Deventer, J.S.J.V. Microstructural changes in alkali activated fly ash/slag geopolymers with sulfate exposure. *Mater. Struct.* **2013**, *46*, 361–373. [CrossRef]
40. Dener, M.; Karatas, M.; Mohabbi, M. Sulfate resistance of alkali-activated slag/Portland cement mortar produced with lightweight pumice aggregate. *Constr. Build. Mater.* **2021**, *304*, 124671. [CrossRef]
41. Ye, H.; Chen, Z.; Huang, L. Mechanism of sulfate attack on alkali-activated slag: The role of activator composition. *Cem. Concr. Res.* **2019**, *125*, 105868. [CrossRef]
42. Bonen, D.; Cohen, M.D. Magnesium sulfate attack on portland cement paste—II. Chemical and mineralogical analyses. *Cem. Concr. Res.* **1992**, *22*, 707–718. [CrossRef]
43. Zhang, J.; Shi, C.; Zhang, Z.; Hu, X. Reaction mechanism of sulfate attack on alkali-activated slag/fly ash cements. *Constr. Build. Mater.* **2022**, *318*, 126052. [CrossRef]
44. Džunuzović, N.; Komljenović, M.; Nikolić, V.; Ivanović, T. External sulfate attack on alkali-activated fly ash-blast furnace slag composite. *Constr. Build. Mater.* **2017**, *157*, 737–747. [CrossRef]
45. Alcamand, H.A.; Borges, P.H.R.; Silva, F.A.; Trindade, A.C.C. The effect of matrix composition and calcium content on the sulfate durability of metakaolin and metakaolin/slag alkali-activated mortars. *Ceram. Int.* **2018**, *44*, 5037–5044. [CrossRef]
46. Gong, K.; White, C.E. Nanoscale chemical degradation mechanisms of sulfate attack in alkali-activated slag. *J. Phys. Chem.* **2018**, *122*, 5992–6004. [CrossRef]
47. Yao, J.; Qiu, H.; He, H.; Chen, X. Application of a Soft Soil Stabilized by Composite Geopolymer. *J. Perform. Constr. Fac.* **2021**, *35*, 04021018. [CrossRef]
48. Kaur, M.; Singh, J.; Kaur, M. Synthesis of fly ash based geopolymer mortar considering different concentrations and combinations of alkaline activator solution. *Ceram. Int.* **2018**, *44*, 1534–1537. [CrossRef]
49. Mithun, B.M.; Narasimhan, M.C. Performance of alkali activated slag concrete mixes incorporating copper slag as fine aggregate. *J. Clean. Prod.* **2016**, *112*, 837–844. [CrossRef]